High-resolution measurement of the electron affinity of cesium

José E. Navarro Navarrete,[1,*] Miranda Nichols,[2] Annie Ringvall-Moberg,[2] Jakob Welander,[2] Di Lu,[2] David Leimbach,[2] Moa K. Kristiansson,[1] Gustav Eklund,[1] Meena Raveesh,[3] Ruslan Chulkov,[4] Vitali Zhaunerchyk,[2] and Dag Hanstorp[2]

[1]*Department of Physics, Stockholm University, SE-106 91 Stockholm, Sweden*
[2]*Department of Physics, University of Gothenburg, SE-412 96 Gothenburg, Sweden*
[3]*International School of Photonics, Cochin University of Science and Technology, Kochi, Kerala 682022, India*
[4]*Department of Physics and Astronomy, Uppsala University, SE-751 20, Box 516, Uppsala, Sweden*

(Received 15 December 2023; accepted 30 January 2024; published 21 February 2024)

Negative ions are unique quantum systems where electron correlation plays a decisive role in determining their properties. The lack of optically allowed transitions prevents traditional optical spectroscopy and the electron affinity is, therefore, for most elements, the only atomic quantity that can be determined with high accuracy. In this work, we present a high-precision experimental determination of the electron affinity of cesium. A collinear laser-ion beam apparatus was used to investigate the partial photodetachment cross section for the cesium anion, leaving the neutral atom in the $6p\,^2P_{3/2}$ excited state. A resonance ionization scheme was used to obtain final-state selectivity, which enabled the investigation of a sharp onset of the cross section associated with a Wigner s-wave threshold behavior. The electron affinity was determined to be 0.471 598 3(38) eV.

DOI: 10.1103/PhysRevA.109.022812

I. INTRODUCTION

Negative ions have a unique structure that differs from their neutral and positive counterparts due to the nature of their creation. The Coulomb potential experienced by the valence electron in neutral atoms and positive ions is proportional to $1/r$, a long-range attraction that allows an infinite series of bound so-called Rydberg states. In negative ions, on the contrary, the bond is governed by an induced dipole potential which arises from the polarization of the atomic core by the additional electron. This potential, scaling as $1/r^4$, is normally too shallow to support any electronically excited states. The lack of a long-range Coulomb interaction between the extra electron and the neutral atom leads to an enhanced importance of electron-electron correlation, which hence plays a crucial role in determining the structure and dynamics of negative ions. Therefore, studies of negative ions can be used as a probe to test theories beyond the independent-particle model which assumes the electrons to move independently in an average potential. Comprehensive overviews of negative ions can be found in reviews such as Pegg *et al.* [1], Andersen *et al.* [2], and Fano [3]. As a consequence of the shallow binding potential and lack of optically allowed transitions, the electron affinity (EA), which is the energy gained by attaching an electron to a neutral atom, is the only quantity that can be experimentally determined with high precision. Typically, this is done utilizing the photodetachment process, where a photon with sufficient energy is used to detach an electron from a negative ion. By tuning the photon energy in a small range around the onset of the process, where the cross section of photodetachment is following the Wigner law [4], the EA can then be extracted [5] by either detecting the resulting neutral atom, as in the case of laser photodetachment threshold spectroscopy (LPTS) (e.g., [6]), or the detached photoelectron, as in the case of laser photodetachment electron spectroscopy (LPES) [7] and laser photodetachment microscopy (LPM) (e.g., [8,9]). The most precise experimental determination of any EA value to date is the recent LPTS study of ^{16}O performed at the DESIREE storage ring [10]. If the energy of the absorbed photon is sufficiently large, the atom produced in the photodetachment process can be left in an excited state. The probability for this to occur is given by the partial photodetachment cross section. By measuring the partial cross section instead of the total cross section, one can obtain detailed information about doubly excited states [11–13] as well as threshold behaviors [14]. Such measurements require a highly sensitive detection method due to the relatively small branching into a single excited state [15], but have shown to be feasible by combining laser photodetachment with resonance ionization spectroscopy (RIS) [16–19]. This method has been applied in several studies of the alkali metal negative ions, including many observations of doubly excited states (e.g., [18,20]).

Cesium (Cs) is the heaviest naturally occurring alkali metal and possesses a single stable isotope, ^{133}Cs. Neutral Cs atoms are among the most studied in atomic physics where they have been of interest for laser cooling [21], studies of Bose-Einstein condensation [22] and atomic clocks [23]. Cesium is also used for the production of negative ion beams by charge exchange processes [24] and as a mean to enhance the production of H^-/D^-, in particular for highly intense

*jose.navarrete@fysik.su.se

beams used for heating in fusion reactors [25]. The negative ion of cesium has been studied far less than the neutral cesium atom. The first theoretical value of the EA of Cs was published in 1973 by Norcross [26]. They obtained an EA of 0.470 eV by using coupled equations of scattering theory based on semi-empirical effective potentials for the neutral atom. One year later, the first accurate EA measurements of Cs via LPTS and LPES were made by Patterson *et al.* [27], where strong resonances below the $6p\ ^2P_{1,2\ 3/2}$ states were discovered, which strongly affected the photodetachment cross section. Nevertheless, they obtained an EA of 0.470(3) eV and 0.472(3) eV by LPES and LPTS, respectively [27]. In 1978, Slater *et al.* determined the ^2P partial photodetachment cross section of Cs yielding an EA of 0.4715(3) eV [28]. Later on, Cs^- was proposed as a candidate for a stable negative ion with opposite parity bound states, but this was disproven by Scheer *et al.* [29] with the observation of the $Cs^-(6s6p\ ^3P)$ states situated just above the ground state of the atom. This represented the first study to observe low-lying resonances in negative ions using photodetachment spectroscopy. Lindahl *et al.* then further investigated these resonances by extending the photodetachment energy range to higher-lying final states with partial photodetachment cross-section measurements [30]. These experiments also gave rise to a series of theoretical work investigating resonances in the photodetachment spectrum of cesium [31–39]. To date, the most accurate value for the EA of Cs was determined to be 0.471630(25) eV by Hotop and Lineberger using LPTS. However, this value was only reported in their 1985 review [40] with the detailed article about the experiment remaining unpublished. Therefore, the most accurate published value for the EA of Cs is 0.47164(6) eV [29]. Apart from a fundamental interest to facilitate theoretical studies of electron correlation in the negative cesium ion, a precise value of the EA is of utmost importance when studying doubly excited states to distinguish between Feshbach and shape resonances, which are situated below and above the parent state, respectively [41,42]. Hence, it is of great interest to update the current experimental value using modern techniques.

In this paper, we present a sensitive, high-resolution measurement of the EA of Cs by investigating the *s*-wave partial photodetachment cross section using LPTS in combination with RIS at the Gothenburg University Negative Ion and Laser Laboratory (GUNILLA) [43]. Here, a new field ionizer for Rydberg atom detection developed by Welander *et al.* [44] was utilized. The collinear geometry, compared to a crossed beam geometry, allowed an increased sensitivity due to the larger interaction volume as well as mitigation of the Doppler effect. At the same time, the final-state detection provided high selectivity, enabling a more accurate determination of the EA for Cs. Further, by measuring the partial photodetachment threshold, leaving the atom in the excited $6p\ ^2P_{3/2}$ state, we completely circumvented the possible influence of the shape resonance present just above the ground state of the cesium atom.

II. EXPERIMENTAL METHOD

A stable beam of Cs^- was produced in a Middleton type sputter ion source [45] (PS-120 Peabody Scientific) using an aluminium cathode. The ions were accelerated to a kinetic energy of 6 keV and selected by a 90° mass separating magnet with a resolution ($M/\Delta M$) of approximately 500. The Cs^- ions were then deflected with a quadrupole deflector into the Rydberg Atom Detector for Anion Research (RADAR) spectrometer [44], as shown in Fig. 1. Here, the ion beam entered a 70 cm long interaction region where it was overlapped with two different laser beams at wavelengths of λ_1 and λ_2 (as indicated in Fig. 2) which were utilized for photodetachment and subsequent resonance ionization, respectively.

To populate the excited state in the neutral cesium atom, the laser pulse for photodetachment (λ_1) was set to arrive a few ns before the laser pulse for resonance excitation (λ_2), as discussed in detail below. Both photodetached and unaffected products then continued into the field ionization region where an electric field gradient was created by 11 parallel circular electrodes. The electric potentials on the first ten electrodes were set to form a slowly decreasing potential, whereas the 11th electrode was grounded. While the weak electric field in the region of the first ten electrodes did not affect Rydberg atoms, the field between the tenth and 11th electrodes was sufficiently strong to effectively ionize them. The positive ions thus created were then decelerated and exited the field ionizer with a decreased kinetic energy with respect to their initial energy. The electric potential applied to these electrodes, as a function of distance along the ion beam axis inside the field ionizer, is shown in Fig. 1. More detailed information about the field ionizer can be found in [44]. Positive ions created in the interaction region by either collisions with the residual gas or in two-photon ionization processes were, on the contrary, first accelerated and then decelerated in the field ionizer, therefore, departing the field ionizer with the same kinetic energy as they entered with. This energy difference was then used to spatially separate these background events from the signal on the position-sensitive detector, consisting of a stack of two microchannel plates (MCP) and a delay line detector by employing an electrostatic energy analyzer, deflecting the positive ions by about 90°. In addition, the field of the energy analyzer removed the remaining negative ions by deflecting them in the opposite direction, while fast neutral atoms continued on a straight forward trajectory, unaffected by the electric field.

The laser excitation scheme of this experiment is shown in Fig. 2. Negative Cs ions were photodetached by absorbing a photon from a tunable laser operating at λ_1. A second laser was set to a fixed wavelength of λ_2 for the resonant excitation of the neutral atoms from the $6p\ ^2P_{3/2}$ excited state to the $25d\ ^2D_{j=5/2,3/2}$ Rydberg state.

For the photodetachment process a Sirah PrecisionScan dye laser was used with a solution of DCM dye in dimethyl sulfoxide (DMSO) to generate photons in the 636 nm to 680 nm range, monitored with a HighFinesse WS6-600 wavelength meter with an accuracy of 600 MHz (2.5 μeV). The linewidth of the dye laser was specified by the manufacturer to be 0.075 cm^{-1} (9.3 μeV) with a pulse energy of about 1.7 mJ. An optical parametric oscillator (OPO) with a bandwidth smaller than 0.2 cm^{-1}, with a pulse energy of 100 μJ, provided photons of 514 nm for the resonant excitation. The dye laser and the OPO were pumped by two different pulsed Nd:YAG lasers with a repetition rate of 10 Hz, respectively. The

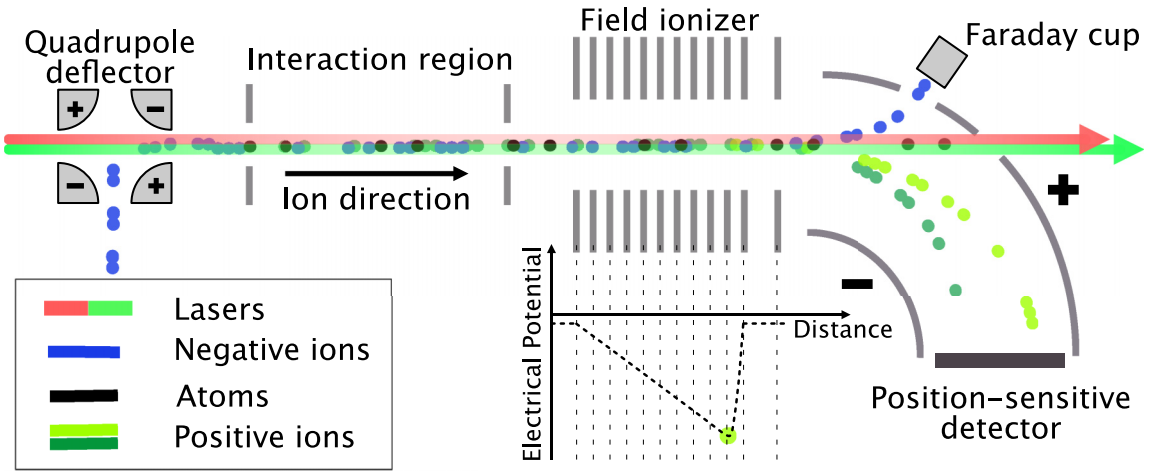

FIG. 1. A schematic figure of the RADAR spectrometer. Negative ions were deflected into the interaction region by a quadrupole deflector where they were overlapped with two laser beams. Downstream of the interaction region is a field ionizer where Rydberg atoms were field ionized. The ions and atoms were then separated by their charge and energy. Neutral atoms continued in a straight path, whereas charged particles were deflected by an energy analyzer. While negative ions were deflected into a Faraday cup, positive ions were guided onto a position-sensitive detector, where the impact position was dependent on their kinetic energy.

duration of the laser pulses was about 8 ns and 5 ns for λ_1 and λ_2, respectively.

The time difference between the pulses was set to maximize the atomic population in the intermediate $6p\ ^2P_{3/2}$ state, which was slightly different depending on the propagation scheme (co or counterpropagating ion and laser beams). The data acquisition was triggered 4.3 μs after the OPO pulse (λ_2) to match the ion time of flight from the end of the interaction region of the RADAR spectrometer to the position-sensitive detector. The time window for data acquisition was set to correspond to the time of flight within the interaction region. A schematic of this time delay process is shown in Fig. 3.

Finally, we investigate the calibration of our wavelength meter by performing saturated absorption spectroscopy of rubidium gas in a low-pressure quartz cell. The light used in the calibration was of a CW external cavity diode laser centered at 780.24 nm. The hyperfine transitions in the D1 line of both ^{85}Rb and ^{87}Rb were measured and compared with tabulated values [46]. The average difference between our measured and the reported values was of 260 MHz. We could therefore with confidence use the specified accuracy of the wavemeter of 600 MHz as the uncertainty in our wavelength reading (2.5 μeV).

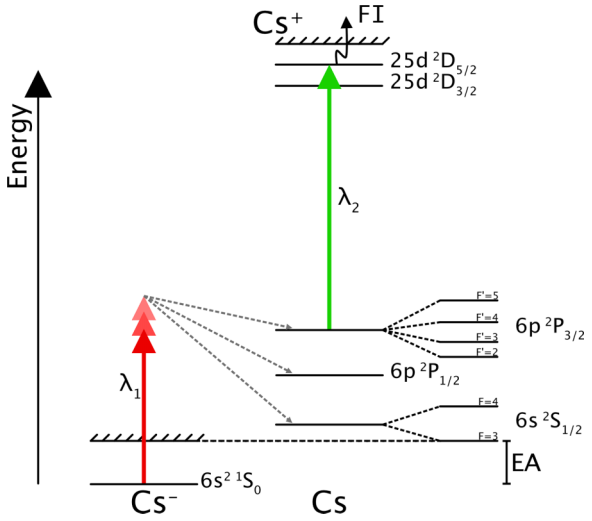

FIG. 2. Partial energy level diagram (not to scale) for Cs^- and Cs. A photon (λ_1) from a frequency tunable laser is absorbed by a Cs^- ion (red arrows). Subsequently, the ion can decay into three different neutral states via electron emission (dashed arrows). The neutral Cs atom in the $6p\ ^2P_{3/2}$ excited state then absorbed another photon (λ_2) at a fixed wavelength for resonant excitation to the Rydberg state, $25d\ ^2D_{5/2}$ (green arrow). Finally, the Rydberg atom underwent a field ionization (F.I.) process (curved arrow), creating a positive ion.

III. RESULTS AND DISCUSSION

As a first step, a two-dimensional (2D) histogram of the signal's spatial distribution was recorded on the position-

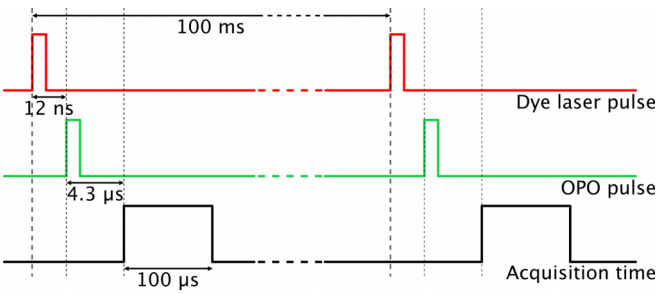

FIG. 3. Time delay and data acquisition scheme (not to scale). The signal from the dye laser pulse initialized the cycle. The delay between the dye laser and the OPO pulses was optimized to be a few ns with slightly different values for co and counterpropagating laser and ion beams, respectively. The acquisition time was triggered 4.3 μs after the OPO laser pulse, corresponding to the time of flight from the interaction region to the detector. The entire measurement cycle was 100 ms.

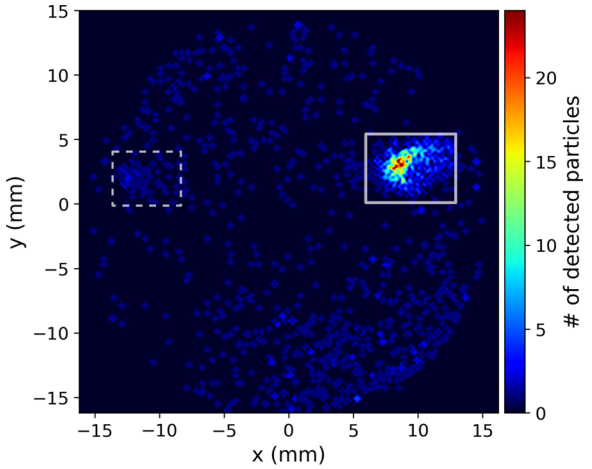

FIG. 4. Two-dimensional histogram of the events measured with the position-sensitive detector. The detector surface is shown from the perspective of the impinging ions. The signal surrounded by the solid rectangle corresponds to events associated with positive ions created by field ionization. The small signal to the left, surrounded by a dashed rectangle, corresponds to the background which consist of the positive ions produced by double photoionization and collisions with the residual gas.

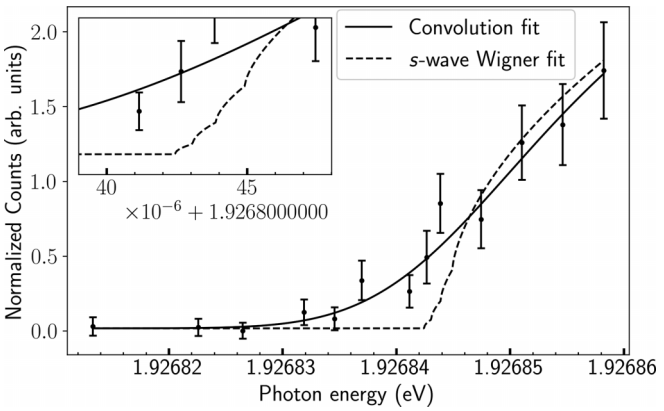

FIG. 5. The number of registered events following the Doppler-shifted partial photodetachment that leaves the neutral atom in the excited state $6p\ ^2P_{3/2}, F = 2$ state, as a function of the photon energy. Both the ion beam and the laser (λ_1) were merged in a copropagating scheme. The fit was obtained with Eq. (1) and is shown as a solid line. The optimized parameters were then used in Eq. (3) to obtain a deconvoluted *s*-wave Wigner function that is shown as a dashed line. The threshold for this measurement is 1.926 842 4(51) eV. The inset shows an expansion around the threshold where the hyperfine structure of the excited state is resolved.

sensitive detector, as shown in Fig. 4. Here, λ_1 was set to a photon energy well above the photodetachment threshold, while (λ_2) was set to be in resonance with the $25d\ ^2D_{j=5/2,3/2}$ Rydberg state. The orientation of the MCP is shown from the ion's reference frame. The signal, delimited by the solid rectangle to the right, corresponds to the positive ions created inside the field ionizer. The number of signal counts inside the solid rectangle is proportional to the partial photodetachment cross section, leaving the neutral atom in the $6p\ ^2P_{3/2}$ state. Background events such as positive ions created by two-photon ionization by absorbing two λ_2 photons or by collisions with the residual gas impinged on the left side of the MCP, within the dashed rectangle. Particles detected outside these two regions correspond to scattered particles or light or result from dark counts of the detector.

A representative plot of the measured *s*-wave Doppler-shifted photodetachment cross section of the Cs negative ions is presented in Fig. 5. In this measurements, (λ_2) was fixed to the frequency of the $6p\ ^2P_{3/2} \rightarrow 25d\ ^2D_{5/2}$ transition and (λ_1) was scanned over the threshold region. In this case, both laser beams were merged copropagating as shown in Fig. 1. Each data point corresponds to the integrated number of positive ions inside the region delimited by the solid rectangle in Fig. 4. These values were then normalized to both the ion current and the laser pulse energy. The uncertainty of the signal was determined as the square root of the total number of counts, as each detected event is a process that follows a Poisson distribution. The final uncertainty of each data point was obtained by Gaussian error propagation.

A deconvolution technique was applied to account for the influence of the bandwidth of the laser and the velocity spread of the ions. Furthermore, there are four photodetachment thresholds with slightly different energies corresponding to the four hyperfine levels in $6p\ ^2P_{3/2}$ state of the neutral Cs atom. Therefore, the experimental data was fitted with the mathematical expression

$$(\sigma \circledast g)(E_n) = \sum_{E_m} \sigma(E_m) g(E_n - E_m), \tag{1}$$

which is a discrete convolution between the Gaussian normalized function

$$g(E_n - E_m) = \left(\frac{1}{\sigma_g \sqrt{2\pi}}\right) e^{-(E_n - E_m)^2/(2\sigma_g^2)} \tag{2}$$

and the Wigner function

$$\sigma(E_m) = A + B \sum_{F=2}^{5} (2F+1) \times (E_m - E_{\mathrm{Th}F})^{l+1/2} \Theta(E_m - E_{\mathrm{Th}F}). \tag{3}$$

Here, E_m is the photon energy, $E_{\mathrm{Th}F} = E_{\mathrm{Th}} + E_F$ is the sum of the photodetachment threshold energy E_{Th} and the energy of the hyperfine level F relative to the $6p\ ^2P_{3/2}$ ($F = 2$) state. This means that E_{Th} is the Doppler-shifted threshold energy where the atom is left in the lowest hyperfine level ($F = 2$) of the excited $6p\ ^2P_{3/2}$ state. All four hyperfine levels are shown schematically in Fig. 2 and the energetic differences were taken from Tanner and Wieman [47]. The corresponding terms were added and the multiplicity of every level was taken into account, following the angular coupling derivation of Peláez *et al.* [48], where the amplitude of the different channels are shown to be proportional to $(2F + 1)$. Here l is the angular momentum of the detached electron, which in this case is $l = 0$. Moreover, the Heaviside function Θ acounts for the zero cross section of photodetachment below the threshold. E_{Th}, A, B, and σ_g are the parameters that were optimized using a least square fitting algorithm. The number of terms in the sum of Eq. (1) was chosen to make the numerical bias negligible. In

this particular case, as shown in Fig. 5, the fit of the experimental data yields a value of $E_{\mathrm{Th}} = 1.926\,842\,4(51)$ eV, where the uncertainty is the statistical error of the fit. The parameter σ_g describes the contribution of the linewidth of the laser (λ_1) and the energy spread of the ions in the convolution. An average σ_g from 15 threshold scans was determined from the statistical fit to be 6.2(7) μeV, which translates to a FWHM of 14.6(16) μeV. This sets the limit of the experimental resolution determined by a convolution of the effect of the laser linewidth and the energy spread of the negative ion beam.

To cancel out the Doppler shift effect to all orders, measurements were alternated between co and counterpropagation schemes and then calculate the geometrical mean

$$E_{\mathrm{Th}}^{\mathrm{Corr}} = (E_{\mathrm{Th}}\uparrow\uparrow E_{\mathrm{Th}}\uparrow\downarrow)^{1/2}. \tag{4}$$

The analytical treatment of our data is exemplified as follows: The data presented in Fig. 5 was measured in a copropagating scheme. The corresponding counterpropagating threshold was determined to be 1.925 644 4(44) eV. By applying Eq. (4), a value corrected for the Doppler shift of 1.926 243 3 (34) eV was obtained. From a series of 15 measurements, switching back and forth between the co and counterpropagating schemes, a weighted average of the geometrical mean yields a value of 1.926 239 0(10) eV. To extract the EA, the difference in energy between the ground state $6s\ ^2S_{1/2}(F = 3)$ and the excited state $6p\ ^2P_{3/2}$ $(F = 2)$ of the neutral Cs atom was subtracted from the corrected $E_{\mathrm{Th}}^{\mathrm{Corr}}$ mean values. Udem *et al.* [49] determined this energy difference in an absolute optical frequency measurement using a frequency comb. Their experimental value and uncertainty was given as the transition frequency expressed in Hz. By using the 2018 CODATA [50] this value can be converted to an energy of 1.454 640 672 0(5) eV. A preliminary electron affinity of Cs of 0.471 598 3(9) eV is obtained, with an error bar which is only statistical. This statistical uncertainty include the effects of the energy spread of the ions, the linewidth of the laser and the divergence of both the laser and ion beams.

Next we consider systematic errors in the experiment. First, we estimated the size of the Ponderomotive shift caused by a strong electromagnetic laser field. For this we measured an average pulse energy of 1.7 mJ and a pulse length of 8 ns for λ_1. The beam waist was estimated to be ∼3 mm at full width at half maximum (FWHM). This gives a ponderomotive energy shift of 0.02 μeV in the threshold measurement. Another possible source of error, is a difference in the interception angle between the co and counterpropagating geometries (which was estimated to be 0.01 μeV, as limited by the apertures in the interaction region, following the procedure of Hanstorp [51]). Moreover, we also considered a possible drift in the kinetic energy of the ions due to fluctuations in the power supplies. According to the specifications, their stability translates into a 0.1% peak to peak ripple. This means that the drift accounts to 6 V. This is equivalent to a Doppler shift variation of 300 neV. We therefore conclude that the greatest source of uncertainty stems from the accuracy and calibration of our wavelength meter (2.5 μeV). By adding up this later error, the shift from the Ponderomotive effect (0.02 μeV), the uncertainty due to the interceptions of the ion and laser beams (0.01 μeV), a kinetic ion beam drift (0.3 μeV), and the statistical error (1 μeV), a final value of 0.471 598 3(38) eV was obtained. This reduces the uncertainty of the electron affinity of Cesium by an order of magnitude in comparison to the value of 0.471 630(25) eV reported in [40] by Hotop and Lineberger. This is largely due to the state-selective method which resulted in a sharp *s*-wave behavior in combination with a high signal-to-background ratio. As shown in Fig. 6, this EA value coincides with our value within their error bars. When comparing with the value of 0.471 630(25) eV as presented by Hotop and Lineberger [40], we find that our value lies slightly outside their uncertainty. However, this can be explained by the fact that they did not take into account the hyperfine structure of the ground state of the Cs atom. This leads to an overestimation in their EA of 21 μeV, which is the difference between the "*center of gravity*" of the $6s\ ^2S_{1/2}$ hyperfine doublet and the lowest hyperfine state ($F = 2$). With this difference taken into account, their value agrees with ours within their error bars (Fig. 6). Finally, the EA of Cesium of 0.471593(36) eV from our previous work [44] is in agreement with our present value.

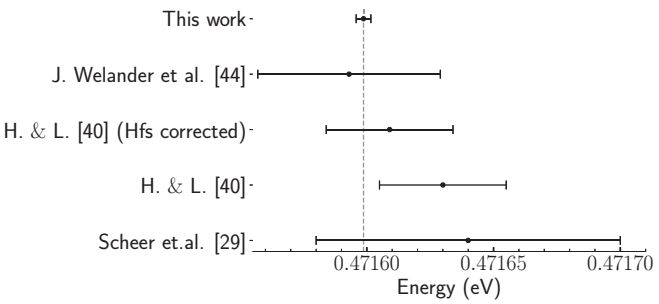

FIG. 6. The experimental value for the EA of this work is shown with a diamond marker. The error bar of this measurement is, within the resolution in this figure, almost imperceptible. The values from Hotop and Lineberger (H. and L.) and its hyperfine splitting correction of 21 μeV [40], Scheer *et al.* [29] and J. Welander *et al.* [44] are shown for comparison.

IV. CONCLUSION AND OUTLOOK

We determined the electron affinity of cesium to be 0.471 598 3(38) eV, obtaining an improvement of one order of magnitude in the uncertainty from the value reported in [40]. This was accomplished by combining laser photodetachment threshold spectroscopy with resonance ionization to investigate the partial photodetachment cross section between the ground state of Cs^- and the $6p\ ^2P_{3/2}$ excited state of the neutral Cs atom. A collinear laser-ion beam geometry allowed us to achieve high sensitivity due to the large area of interaction as well as high resolution due to Doppler shift mitigation by making use of both co and counterpropagating laser-ion beam configurations. Our experimental method made use of a field ionizer developed by Welander *et al.* [44], specifically designed for partial photodetachment cross-section studies. The apparatus allowed for a highly selective detection method which facilitated the detection of a single photodetachment channel. This made it possible for us to detect the $6p\ ^2P_{3/2}$ photodetachment channel, which yields a sharp onset of the cross section associated with a Wigner *s*-wave threshold behavior, on the contrary to previous experiments where the

slow onset of a p-wave threshold obtained when leaving the neutral atom in the ground state was investigated. Further, detection of the $6p\ ^2P_{3/2}$ channel circumvented the possible problem with the resonance situated just above the ground state of the neutral atom. It is our hope that this precise measurement will trigger new theoretical calculations of the EA of Cs. This should be tractable since it has a closed $6s^2$ valence shell.

The presented experimental method can also be applied to study other alkali metals, such as rubidium and francium. Francium, the heaviest homologue to Cs, possesses no stable isotope and has an EA which is experimentally unknown, but is predicted to be between 0.475 eV [52] and 0.491(5) eV [35]. Determining this would complete the EA measurements for the alkali metal group and could help us understand more about electron correlations and relativistic effects of heavy elements. Francium, a near-actinide element, can be studied in a facility that can produce radioactive ion beams, such as ISOLDE at CERN [53]. At this facility it has been shown that it is possible to measure electron affinities of radioactive isotopes, where the EA of ^{128}I [54] and ^{211}At [6] were measured. Combining the abilities of a facility such as ISOLDE with the method used in this paper will allow a determination of the EA of francium in the near future. In addition, studies of near-actinides will pave the way for future studies of negative ions of actinides, for which very little is known.

The supporting data for this article is openly available from the Zenodo data repository [55].

ACKNOWLEDGMENTS

Financial support from the Swedish Research Council (Grants No. 2016-03650 and No. 2020-03505) is acknowledged. This project has received funding from the European Union's Horizon 2020 research and innovation program under the Marie Skodowska-Curie Grant Agreement No. 861198.

[1] D. J. Pegg, Rep. Prog. Phys. **67**, 857 (2004).
[2] T. Andersen, Phys. Rep. **394**, 157 (2004).
[3] U. Fano, Rep. Prog. Phys. **46**, 97 (1983).
[4] E. P. Wigner, Phys. Rev. **73**, 1002 (1948).
[5] T. Andersen, H. K. Haugen, and H. Hotop, J. Phys. Chem. Ref. Data **28**, 1511 (1999).
[6] D. Leimbach, J. Karls, Y. Guo, R. Ahmed, J. Ballof, L. Bengtsson, F. Boix Pamies, A. Borschevsky, K. Chrysalidis, E. Eliav *et al.*, Nat. Commun. **11**, 3824 (2020).
[7] R. Tang, Y. Lu, H. Liu, and C. Ning, Phys. Rev. A **103**, L050801 (2021).
[8] C. Blondel, C. Delsart, F. Dulieu, and C. Valli, Eur. Phys. J. D, **5**, 207 (1999).
[9] C. Blondel, C. Delsart, and F. Goldfarb, J. Phys. B: At. Mol. Opt. Phys. **34**, 281 (2001).
[10] M. K. Kristiansson, K. Chartkunchand, G. Eklund, O. M. Hole, E. K. Anderson, N. de Ruette, M. Kamińska, N. Punnakayathil, J. E. Navarro-Navarrete, S. Sigurdsson, J. Grumer, A. Simonsson, M. Björkhage, S. Rosén, P. Reinhed, M. Blom, A. Källberg, J. D. Alexander, H. Cederquist, H. Zettergren *et al.*, Nat. Commun. **13**, 5906 (2022).
[11] A. O. Lindahl, J. Rohlén, H. Hultgren, I. Y. Kiyan, D. J. Pegg, C. W. Walter, and D. Hanstorp, Phys. Rev. A **85**, 033415 (2012).
[12] I. Y. Kiyan, U. Berzinsh, D. Hanstorp, and D. J. Pegg, Phys. Rev. Lett. **81**, 2874 (1998).
[13] P. G. Harris, H. C. Bryant, A. H. Mohagheghi, R. A. Reeder, C. Y. Tang, J. B. Donahue, and C. R. Quick, Phys. Rev. A, **42**, 6443 (1990).
[14] J. Rohlén, A. O. Lindahl, H. Hultgren, R. D. Thomas, D. J. Pegg, and D. Hanstorp, Europhys. Lett. **106**, 53001 (2014).
[15] C.-N. Liu and A. F. Starace, Phys. Rev. A **59**, 3643 (1999).
[16] H. H. Andersen, V. V. Petrunin, P. Kristensen, and T. Andersen, Phys. Rev. A **55**, 3247 (1997).
[17] V. V. Petrunin, H. H. Andersen, P. Balling, and T. Andersen, Phys. Rev. Lett. **76**, 744 (1996).
[18] G. Haeffler, D. Hanstorp, I. Kiyan, A. E. Klinkmüller, U. Ljungblad, and D. J. Pegg, Phys. Rev. A **53**, 4127 (1996).
[19] P. Kristensen, U. V. Pedersen, V. V. Petrunin, T. Andersen, and K. T. Chung, Phys. Rev. A **55**, 978 (1997).
[20] G. Haeffler, I. Y. Kiyan, D. Hanstorp, B. J. Davies, and D. J. Pegg, Phys. Rev. A **59**, 3655 (1999).
[21] D. Zhang, Y. Q. Li, Y. F. Wang, Y. M. Fu, P. Li, W. L. Liu, J. Z. Wu, J. Ma, L. T. Xiao, and S. T. Jia, Chin. Phys. B **29**, 023203 (2020).
[22] T. Kraemer, J. Herbig, M. Mark, T. Weber, C. Chin, H. C. Nägerl, and R. Grimm, Appl. Phys. B **79**, 1013 (2004).
[23] R. J. Hendricks, F. Ozimek, K. Szymaniec, B. Nagorny, P. Dunst, J. Nawrocki, S. Beattie, B. Jian, and K. Gibble, IEEE Trans. Ultrason. Ferroelectr. Freq. Control **66**, 624 (2019).
[24] M. Bacal, A. Truc, H. J. Doucet, H. Lamain, and M. Chrétien, Nucl. Instrum. Methods **114**, 407 (1974).
[25] A. Ando, Y. Takeiri, K. Tsumori, O. Kaneko, Y. Oka, R. Akiyama, T. Kawamoto, K. Mineo, T. Kurata, and T. Kuroda, Rev. Sci. Instrum. **63**, 2683 (1992).
[26] D. W. Norcross, Phys. Rev. Lett. **32**, 192 (1974).
[27] T. A. Patterson, H. Hotop, A. Kasdan, D. W. Norcross, and W. C. Lineberger, Phys. Rev. Lett. **32**, 189 (1974).
[28] K. J. Slater, F. H. Readt, S. E. Novick, and W. C. Lineberger, Phys. Rev. A **17**, 201 (1978).
[29] M. Scheer, J. Thøgersen, R. C. Bilodeau, C. A. Brodie, H. K. Haugen, H. H. Andersen, P. Kristensen, and T. Andersen, Phys. Rev. Lett. **80**, 684 (1998).
[30] A. O. Lindahl, J. Rohlén, H. Hultgren, D. J. Pegg, C. W. Walter, and D. Hanstorp, Phys. Rev. A **88**, 053410 (2013).
[31] C. H. Greene, Phys. Rev. A **42**, 1405 (1990).
[32] C. Bahrim and U. Thumm, Phys. Rev. A **61**, 022722 (2000).
[33] C. H. Greene, A. S. Dickinson, and H. R. Sadeghpour, Phys. Rev. Lett. **85**, 2458 (2000).
[34] C. Bahrim, I. I. Fabrikant, and U. Thumm, Phys. Rev. Lett. **87**, 123003 (2001).
[35] A. Landau, E. Eliav, Y. Ishikawa, and U. Kaldor, J. Chem. Phys **115**, 2389 (2001).

[36] C. Bahrim, U. Thumm, A. A. Khuskivadze, and I. I. Fabrikant, Phys. Rev. A **66**, 052712 (2002).
[37] A. A. Khuskivadze, I. I. Fabrikant, and U. Thumm, Phys. Rev. A **68**, 063405 (2003).
[38] A. Z. Msezane, Z. Felfli, and D. Sokolovski, Chem. Phys. Lett. **456**, 96 (2008).
[39] J. Li, Z. Zhao, and X. Zhang, Europhys. Lett. **107**, 33001 (2014).
[40] H. Hotop and W. C. Lineberger, J. Phys. Chem. Ref. Data **14**, 731 (1985).
[41] K. T. Andersson, J. Sandström, I. Y. Kiyan, D. Hanstorp, and D. J. Pegg, Phys. Rev. A **62**, 022503 (2000).
[42] I. Y. Kiyan, U. Berzinsh, J. Sandström, D. Hanstorp, and D. J. Pegg, Phys. Rev. Lett. **84**, 5979 (2000).
[43] C. Diehl, K. Wendt, A. O. Lindahl, P. Andersson, and D. Hanstorp, Rev. Sci. Instrum. **82**, 053302 (2011).
[44] J. Welander, J. E. N. Navarrete, J. Rohlén, T. Leopold, R. D. Thomas, D. J. Pegg, and D. Hanstorp, Rev. Sci. Instrum. **93**, 065004 (2022).
[45] R. Middleton, Nucl. Instrum. Methods Phys. Res. **214**, 139 (1983).
[46] G. P. Barwood, P. Gill, and W. R. Rowley, Appl. Phys. B **53**, 142 (1991).
[47] C. E. Tanner and C. Wieman, Phys. Rev. A **38**, 1616 (1988).
[48] R. J. Peláez, C. Blondel, C. Delsart, and C. Drag, J. Phys. B: At. Mol. Opt. Phys. **42**, 125001 (2009).
[49] T. Udem, J. Reichert, T. W. Hänsch, and M. Kourogi, Phys. Rev. A **62**, 031801(R) (2000).
[50] E. Tiesinga, P. Mohr, D. Newell, and B. Taylor, Rev. Mod. Phys. **93**, 025010 (2021).
[51] D. Hanstorp, Nucl. Instrum. Methods Phys. Res. Sect. B **100**, 165 (1995).
[52] J. G. Hill and K. A. Peterson, J. Chem. Phys. **147**, 244106 (2017).
[53] R. Catherall, W. Andreazza, M. Breitenfeldt, A. Dorsival, G. J. Focker, T. P. Gharsa, T. J. Giles, J. L. Grenard, F. Locci, P. Martins, S. Marzari, J. Schipper, A. Shornikov, and T. Stora, J. Phys. G: Nucl. Part. Phys. **44**, 094002 (2017).
[54] S. Rothe, J. Sundberg, J. Welander, K. Chrysalidis, T. D. Goodacre, V. Fedosseev, S. Fiotakis, O. Forstner, R. Heinke, K. Johnston, T. Kron, U. Köster, Y. Liu, B. Marsh, A. Ringvall-Moberg, R. E. Rossel, C. Seiffert, D. Studer, K. Wendt, and D. Hanstorp, J. Phys. G: Nucl. Part. Phys. **44**, 104003 (2017).
[55] J. E. N. Navarrete, M. Nichols, and A. Ringvall-Moberg, Zenodo (2023), doi:10.5281/zenodo.10184936.